Journal of Inorganic Biochemistry 199 (2019) 110777

Contents lists available at ScienceDirect

Journal of Inorganic Biochemistry

journal homepage: www.elsevier.com/locate/jinorgbio

Focused review

Catalytic recycling of NAD(P)H

Shunichi Fukuzumi[a,b,*], Yong-Min Lee[a,c,*], Wonwoo Nam[a,d,*]

[a] Department of Chemistry and Nano Science, Ewha Womans University, Seoul 03760, Republic of Korea
[b] Faculty of Science and Engineering, Meijo University, Nagoya, Aichi 468-8502, Japan
[c] Research Institute for Basic Sciences, Ewha Womans University, Seoul 03760, Republic of Korea
[d] State Key Laboratory for Oxo Synthesis and Selective Oxidation, Suzhou Research Institute of LICP, Lanzhou Institute of Chemical Physics (LICP), Chinese Academy of Sciences, Lanzhou 730000, China

ARTICLE INFO

Keywords:
$NAD(P)^+$
NAD(P)H
Redox catalysis
Metal hydride complexes
Electron transfer

ABSTRACT

A large number of industrially relevant enzymes depend upon dihydronicotinamide adenine dinucleotide (NADH) and dihydronicotinamide adenine dinucleotide phosphate (NADPH) cofactors, which are too expensive to be added in stoichiometric amounts. Existing NAD(P)H-recycling systems suffer from low activity, or the generation of side products. This review focuses on NAD(P)H cofactor regeneration catalyzed by transition metal complexes such as rhodium, ruthenium and iridium complexes using cheap reducing agents such as hydrogen (H_2) and ethanol, which have attracted increasing attention as sustainable energy carriers. The catalytic mechanisms for the regioselective reduction of $NAD(P)^+$ are discussed with emphasis on identification of catalytically active intermediates such as transition metal hydride complexes. Applications of NAD(P)H-recycling systems to develop artificial photosynthesis are also discussed.

1. Introduction

Oxidoreductases play central roles in metabolic processes, such as photosynthesis, respiration, the degradation of carbohydrates, and the reduction of carbonyl groups, acids, C=C double bonds, nitro groups, and C-N multiple bonds, representing about one-fourth of all known enzymes [1–5]. In particular, monooxygenases catalyze a variety of oxyfunctionalization reactions under very mild conditions, thus being a focus of significant attention as promising candidates for environmentally benign catalysts in practical applications [6–9]. However, monooxygenases, such as cytochrome P450s, require a stoichiometric amount of expensive cofactors (e.g., NAD(P)H) as electron and proton donors to produce catalytically active species, such as high-valent metal-oxo species, which have hindered further in vitro application of these enzymes [10–14]. Thus, extensive efforts have been devoted to the development of efficient methods for regeneration of NADP(H) from $NAD(P)^+$ (Fig. 1) with inexpensive reducing equivalents in the last decades [15–27]. Methods explored include chemical, electrochemical, and photochemical approaches [15–27]. None of the methods to regenerate NADH has reached an efficiency and selectivity comparable with enzymatic regeneration (e.g., formate dehydrogenase), which remains the method of choice for most practical applications. This review focuses on catalytic regioselective reduction of $NAD(P)^+$ to produce 1,4-dihydronicotinamides (NAD(P)H) using transition metal complexes, such as rhodium, ruthenium, iridium, and iron complexes, as catalysts. The origin of the regioselectivity to afford 1,4-dihydronicotinamides without formation of 1,2- or 1,6-regioisomer is discussed in the catalytic mechanism. The catalytic reduction of NAD^+ to NADH is combined with enzymatic reduction of CO_2 to develop an artificial photosynthetic system.

2. Rhodium complex catalysts

Wienkamp and Steckhan reported for the first time the regioselective electrocatalytic reduction of NAD^+ to 1,4-NADH using $[Rh^I(bpy)_2]^+$ (bpy = 2,2′-bipyridine) as a catalyst [28]. The direct electrochemical reduction of NAD^+ at −1.1 V vs. SCE afforded the NAD dimer, whereas NAD^+ is reduced regioselectively to 1,4-NADH using the electrochemically generated two-electron transfer agent $[Rh^I(bpy)_2]^+$, which is generated cathodically from $[Rh^{III}(bpy)_3]^{3+}$ [28]. In order to increase the electocatalytic activity, a rhodium-based complex, $[Cp^*Rh^{III}(bpy)Cl]^+$ (Cp_* = pentamethylcyclopentadienyl anion), was covalently bonded at the surface of a multiwall carbon nanotube (MWCNT)-functionalized carbon felt electrode (CF-CNT) by combining diazonium electrografting, Huisgen cycloaddition, and metal complexation [29]. As shown in Fig. 2A, the cathodic current measured at −0.7 V vs. Ag/AgCl increased with increasing concentration of NAD^+, but exhibited a saturation behavior when the final

* Corresponding authors at: Department of Chemistry and Nano Science, Ewha Womans University, Seoul 03760, Republic of Korea.
E-mail addresses: fukuzumi@chem.eng.osaka-u.ac.jp (S. Fukuzumi), yomlee@ewha.ac.kr (Y.-M. Lee), wwnam@ewha.ac.kr (W. Nam).

https://doi.org/10.1016/j.jinorgbio.2019.110777
Received 23 May 2019; Received in revised form 12 July 2019; Accepted 12 July 2019
Available online 13 July 2019
0162-0134/ © 2019 Elsevier Inc. All rights reserved.

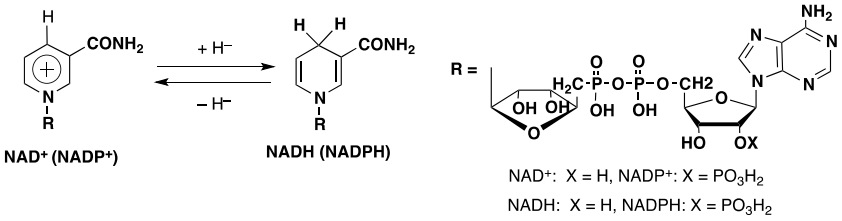

Fig. 1. Chemical structures of NAD(P)$^+$ and NAD(P)H.

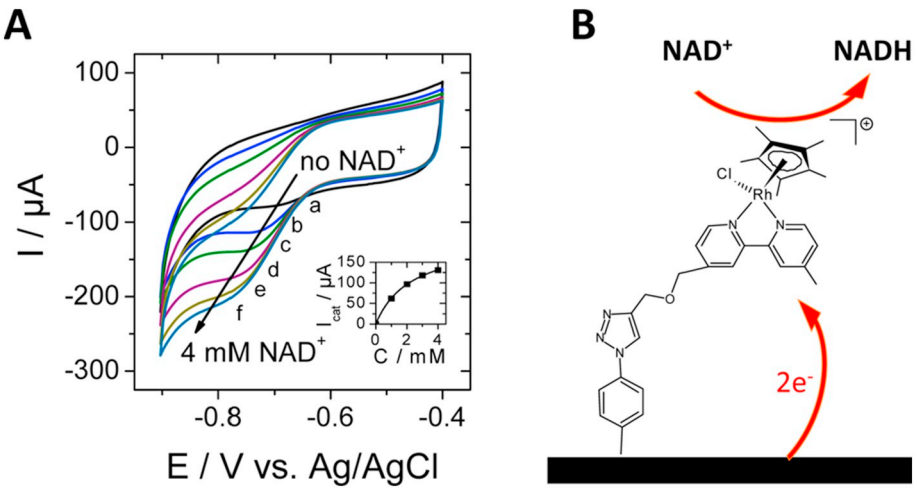

Fig. 2. (A) Cyclic voltammograms recorded at a potential scan rate of 5 mV s^{-1} using a CF-CNT-Rh electrode in 50 mM PBS buffer (pH 6.5), under nitrogen, when NAD$^+$ was added gradually to buffer solution: (a) 0 mM, (b) 0.5 mM, (c) 1 mM, (d) 2 mM, (e) 3 mM, and (f) 4 mM. (B) Schematic representation of NADH regeneration mediated by a CF-CNT-Rh electrode. Reprinted with permission from Ref. [29]. Copyright 2017, American Chemical Society.

concentration of NAD$^+$ reached 4 mM (see inset of Fig. 2A). This behavior is different from that observed when the molecule was in solution, for which a linear increase of the current versus NAD$^+$ concentration was observed in this concentration range [29]. The saturation of the signal with the immobilized complex results from the restricted amount of Rh complexes available associated with limited heterogeneous electron transfer kinetics of the reaction, when the rate constant of the reaction was 0.66 ± 0.07 s^{-1}. The immobilization of the Rh moiety on the electrode (Fig. 2B) provided good stability for the regioselective two-electron reduction of NAD$^+$ to 1,4-NADH in solution under convection over 14 days, which is much better than the simple adsorption of the Rh complex on the electrode surface [29]. Finally, the system was tested in the presence of NAD-dependent dehydrogenases that were immobilized in a sol-gel film on the top of the functionalized porous carbon electrode. A total turnover of 3790 and a turnover frequency of 164 h^{-1} were observed [29].

The covalent immobilization of a rhodium complex mediator ([Cp*Rh(bpy)Cl]$^+$) on the surface of a bucky paper electrode was also achieved by grafting a bipyridine ligand on the electrode followed by electrochemical reduction of bipyridyl diazonium cations generated from 4-amino-2,2′-bipyridine, and the complex was then formed by reaction with $[RhCp^*Cl_2]_2$ [30]. A turnover frequency of 1.3 s^{-1} was estimated for the electrocatalytic regeneration of NADH by this immobilized complex, with a Faraday efficiency of 83% [30]. The bucky paper electrode was then overcoated by a bio-doped porous layer made of glassy fibers with immobilized D-sorbitol dehydrogenase [30]. A turnover frequency of 0.19 s^{-1} for the rhodium complex was observed in the presence of 3 mM D-fructose and a total turnover number of higher than 12,000 was achieved [30].

$[Rh^I(bpy)_2]^+$ can also act an effective catalyst for photocatalytic generation of repairing enzyme-active 1,4-NADH from NAD$^+$ using visible light in the presence of $[Ru^{II}(bpy)_3]^{2+}$ as a photoredox catalyst and 2,2′,2″-nitrilotriethanol (triethanolamine, TEOA) as an electron donor as shown in Scheme 1, where electron transfer from the excited state of $[Ru^{II}(bpy)_3]^{2+*}$ (* denotes the excited state) to $[Rh^{III}(bpy)_3]^{3+}$ occurs to produce $[Ru^{III}(bpy)_3]^{3+}$ and $[Rh^{II}(bpy)_3]^{2+}$ [31]. The disproportionation of $[Rh^{II}(bpy)_3]^{2+}$ affords $[Rh^{III}(bpy)_3]^{3+}$ and $[Rh^I(bpy)_3]^+$, in which the bpy ligand is dissociated to produce $[Rh^I(bpy)_2]^+$. As described above, $[Rh^I(bpy)_2]^+$ can reduce NAD$^+$ regioselectively to yield enzymatically-active NADH [29]. $[Rh^{III}(terpy)_2]^{3+}$ (terpy = 2,2′; 6′,2″-terpyridine) also catalyzes the regiospecific photocatalytic reduction of NAD$^+$ by TEOA to produce 1,4-NADH. However its catalytic activity in the photochemical reaction is 20 times lower than that of $[Cp^*Rh^{III}(bpy)(H_2O)](OTf)_2$ (**2**) ($OTf^- = CF_3SO_3^-$) due to the absence of a ring-slippage mechanism (vide infra) [32].

A catalytic cycle for the regioselective reduction of the NAD$^+$ model compound, 1-benzyl-3-carbamoylpyridinium cation (BNA$^+$), with **2** as a catalyst precursor and sodium formate (HCO_2Na) as a hydride source is shown in Scheme 2, where the reaction of **2** with HCO_2Na affords the Rh(III)-hydride complex, $[Cp^*Rh(bpy)(H)]^+$ (complex A in Scheme 2), through a β-hydrogen elimination reaction to produce CO_2 [32]. The pivotal role of the amide oxygen atom is to coordinate to the Cp*Rh metal center through an open coordination site on the metal center. This open site is generated by the well documented ring-slippage mechanism of the Cp* ring by a change in the coordination mode of this ligand from η^5 to η^3 [33]. This mechanism includes a kinetically favorable six-membered ring transition state (complex B in Scheme 2), which undergoes the regioselective hydride transfer at the C4 position of BNA$^+$ (complex C in Scheme 2) [32]. During this coordination process, the induced electronic effect of the bound carbonyl group may also cause the C4 position to be a more electrophilic site towards hydride transfer [32].

$[Ru^{II}(bpy)_3]^{2+}$ used as a photoredox catalyst for photocatalytic regioselective reduction of NAD$^+$ to 1,4-NADH with $[Rh^{III}(bpy)_3]^{3+}$ can be replaced by recyclable heterogeneous photoredox catalysts [34–40]. For example, a nanoshell with two moieties of α-Fe_2O_3 and carbon (C) is in situ formed on the surface of a g-C_3N_4 (g-C_3N4@α-Fe_2O_3/C) core through calcination of Fe^{3+}/polyphenol-coated melamine to obtain g-C_3N_4@α-Fe_2O_3/C core@shell photocatalysts [41]. The photocatalytic NADH regeneration was then conducted by using g-C_3N_4@α-Fe_2O_3/C as a photoredox catalyst, TEOA as a sacrificial electron donor, a blue LED (100 W, 405 nm) incident light with single wavelength as the light source, and $[Cp^*Rh(bpy)H_2O]^{2+}$ as the redox catalyst to obtain a yield

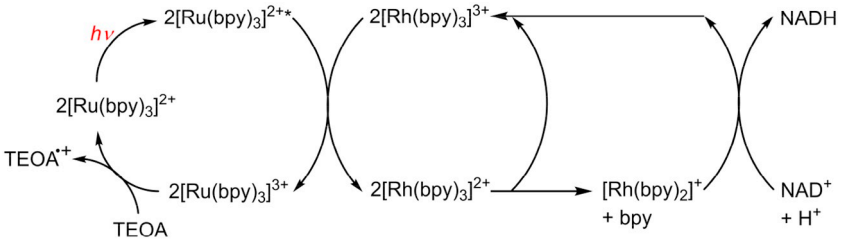

Scheme 1. Catalytic cycles of photocatalytic reduction of NAD^+ by triethanolamine (TEOA) with $[Ru^{II}(bpy)_3]^{2+}$ as a photoredox catalyst and $[Rh^{I}(bpy)_2]^{+}$ as a thermal redox catalyst to produce NADH regioselectively [31].

of 76.3% and an initial reaction rate (r) of 7.7 mmol h^{-1} g^{-1} [41], which was among the highest rate for photocatalytic NADH regeneration [16].

A hybrid glass bead composed of an organometallic rhodium complex containing Cp*Rh moiety as a redox catalyst and a 2,2-bipyridyl-containing poly(arylene-ethynylene)-*alt*-poly(arylene-vinylene) (BipyE-PV*ab*) polymer as a photosensitizer for photocatalytic regioselective reduction of NAD^+ by formate to 1,4-NADH is shown in Fig. 3 [42]. The conversion from NAD^+ to NADH after 26 h compared to the initial amount of NAD^+ was > 21% (8.6 mg NADH l^{-1}), resulting that a turnover number (TON) of 480 μmol cm^{-2} and a turnover frequency (TOF) of 1.8 μmol cm^{-2} h^{-1} were observed using the surface area of the glass beads [42].

Two possible catalytic cycles proposed for the photochemical reduction of NAD^+ to 1,4-NADH by the rhodium-polymer hybrid glass bead, Rh-BipyE-PV*ab*, are shown in Scheme 3 [42]. In the first catalytic cycle, TEOA reductively quenches the excited state of the Rh(III)-complex by photoinduced electron transfer to produce the Rh(II) complex (Scheme 3). The second photoinduced electron transfer from TEOA to the excited state of the Rh(II) complex to produce the Rh(I) complex that reacts with a proton to afford the Rh(III)-hydride complex. Then, a hydride in the Rh(III)-hydride complex is transferred to NAD^+ to yield 1,4-NADH [42]. In the second catalytic cycle (Scheme 3), the rhodium(III) complex oxidatively quenches the excited state of the polymer backbone material BipyE-PV*ab*, which is regenerated by TEOA from the aqueous solution [42]. In this case as well, photoinduced electron transfer from the excited state of the polymer backbone material BipyE-PV*ab* to the Rh complex occurs twice to produce the Rh(I) complex that reacts with a proton to produce the Rh-hydride complex. The coordination of the amide oxygen atom of NAD^+ to the Cp*Rh metal center (Scheme 3) results in the 1,4-selective reduction of NAD^+ to yield 1,4-NADH [42].

3. Ruthenium complex catalysts

The four uncharged tethered Ru^{II} complexes, [Ru(η^6-Ph$(CH_2)_3$-ethylenediamine-N-R)Cl], where R = methanesulfonyl (**1**), toluenesulfonyl (**2**), 4-trifluoromethylbenzenesulfonyl (**3**), and nitrobenzenesulfonyl (**4**) (Fig. 4), exhibited potent catalytic activity for the regioselective reduction of NAD^+ by formate with TOFs of 5.8, 8.3, 8.7, and 9.9 h^{-1}, respectively, to produce 1,4-NADH, following the order **1** < **2** < **3** < **4**. This result suggests that more strongly electron-withdrawing groups on the ethylenediamine moiety facilitate hydride transfer between formate and NAD^+ [43].

A Ru(II) complex, $[Ru^{II}(tpy)(bpy)(NEt_3)]^{2+}$ (tpy = 2,2′:6″,2″-terpyridine), also acts as an efficient photoredox catalyst for the photocatalytic regioselective hydride reduction of BNA^+ (**1a**), which is a typical biomimetic $NAD(P)^+$ model compound (vide supra), using

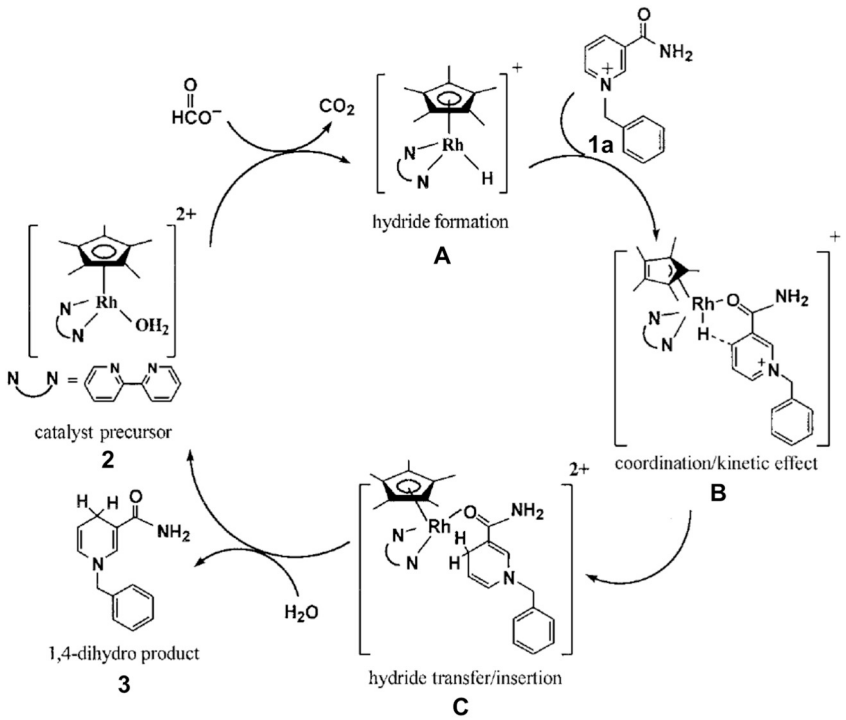

Scheme 2. Proposed mechanism for the catalytic reduction of an NAD^+ model substrate (BNA^+) regioselectively in H_2O-THF (v/v 1:1). Reprinted with permission from Ref. [32]. Copyright 1999, WILEY-VCH Verlag GmbH.

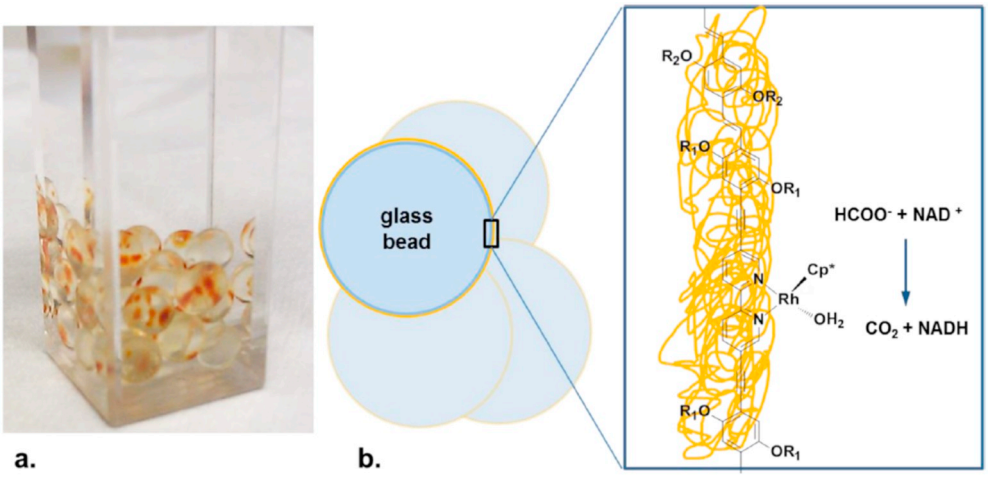

Fig. 3. (a) View of experimental setting. (b) Scheme of the surface reaction using the polymer-bound rhodium catalyst for the reduction of NAD^+ to NADH with sodium formate (HCO_2Na) as a hydride source. Reprinted with permission (CC-BY Licence) from Ref. [42]. Copyright 2014, American Chemical Society.

triethylamine (NEt_3) as a reductant to produce 1,4-BNAH [44–46]. In the beginning of the reaction, the Ru(III)-hydride complex ($[Ru^{III}(tpy)(bpy)H]^+$) is formed via the photoexcitation of $[Ru^{II}(tpy)(bpy)(NEt_3)]^{2+}$ (process 1 in Scheme 4) [46]. The Ru(III)-H complex rapidly reacts with **1a** to give the corresponding the 1:1 adduct **2a**(1,4), which is the carbamoyl group of 1,4-dihydro form **3a**(1,4) (i.e., BNAH) coordinated to the Ru(II) center of $[Ru(tpy)(bpy)]^{2+}$ (process 2 in Scheme 4) [47–49]. **2a**(1,4) quantitatively cleaved at a much slower rate, yielding free **3a**(1,4) (i.e., BNAH), accompanied by regeneration of $[Ru^{II}(tpy)(bpy)(NEt_3)]^{2+}$ (process 3 in Scheme 4) [46]. The observation that the carbamoyl group coordinated to the metal center in the intermediate **2a**(1,4) is the first clear evidence that the interaction between the carbamoyl group and the metal center plays an important role in inducing the regioselective formation of the 1,4-dihydro product, **3a**(1,4) [46]. Because a "seven-coordinated" Ru(II) complex was produced in the transition state (Fig. 5), where the carbamoyl group (or NH_2 group) of **1a** interacts with Ru(II) and the hydride ligand interacts with the C-4 position of the pyridinium unit, the hydride cannot be transferred to the C-6 position, which is much farther than the C-4 position from the carbamoyl group [46]. The hydride ligand did not transfer to the C-2 position of the pyridinium unit of BNA^+ (**1a**) probably due to steric hindrance at the C-2 position [46].

4. Iridium complex catalysts

Regioselective hydrogenation of the oxidized form of β-nicotinamide adenine dinucleotide (NAD^+) with hydrogen molecule (H_2) to the reduced form (1,4-NADH) has been achieved in the presence of a catalytic amount of a [C,N] cyclometalated organoiridium complex, $[Ir^{III}(Cp^*)(4\text{-}(1H\text{-pyrazol-1-yl-}\kappa N^2)\text{benzoic acid-}\kappa C^3)(H_2O)]_2(SO_4)$ ($[\mathbf{1}]_2{\cdot}SO_4$), acting as an efficient redox catalyst under an atmospheric pressure of H_2 in weakly basic water at room temperature [50]. A water-soluble iridium-aqua complex **1** can release protons from the carboxyl group and the aqua ligand to form the corresponding benzoate complex **2** and hydroxo complex **3**, respectively (Fig. 6a) [50]. The pK_a values of complexes **1** and **2** were determined from the spectral titration to be $pK_{a1} = 4.0$ and $pK_{a2} = 9.5$, respectively [50]. The X-ray crystal structure of the benzoate-aqua iridium(III) complex **2** is shown in Fig. 6b, where an uncharged mononuclear iridium(III) species contains no counterions [50]. The iridium-hydride complex was formed under an atmospheric pressure of H_2, undergoing the 1,4-selective hydrogenation of NAD^+ to form 1,4-NADH (Scheme 5) probably via the coordination of the carbamoyl group (or NH_2 group) of NAD^+ to the Ir(III) center and the interaction of the hydride ligand with the C-4 position of NAD^+ as the case of the Ru(II) complex with BNA^+ in Fig. 5 [50]. The same Ir complex and related Ir complexes were reported to catalyze the two-electron reduction of CO_2 to produce formate under basic conditions [51–58].

An Ir(III) complex, [Cp*Ir(pica)Cl] (pica = κ^2-pyridine-2-carboxamide = picolinamidate), was reported to exhibit the higher catalytic activity in the hydrogenation of NAD^+ with potassium formate (HCO_2K) (Scheme 6), leading to the regiospecific formation of 1,4-NADH (at pH 7) with TOF = 143 h^{-1}, which is about 3 times higher than that in Scheme 5 (54 h^{-1}) [59]. Initially, H_2O substitutes Cl^-, leading to complex A, which reacts with HCO_2^- to produce the formate complex B or undergoes a reversible coordination of NAD^+ to afford the iridium-NAD^+ adduct species (E). When the concentration of NAD^+ increases, adduct species E slows down the catalytic reduction of NAD^+ [59]. The formation of complex B is favored by a hydrogen bond interaction between the oxygen atom of the carboxylic moiety and

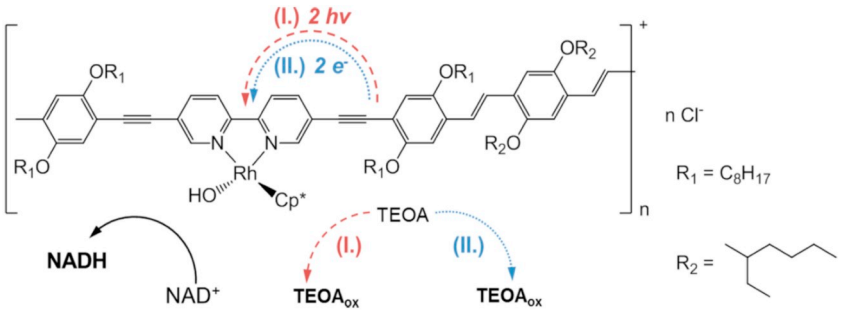

Scheme 3. Proposed mechanism for the catalytic reduction of an NAD^+ regioselectively to 1,4-NADH by TEOA with the rhodium-polymer hybrid glass bead, Rh-BipyE-PV*ab*. Reprinted with permission (CC-BY Licence) from Ref. [42]. Copyright 2014, American Chemical Society.

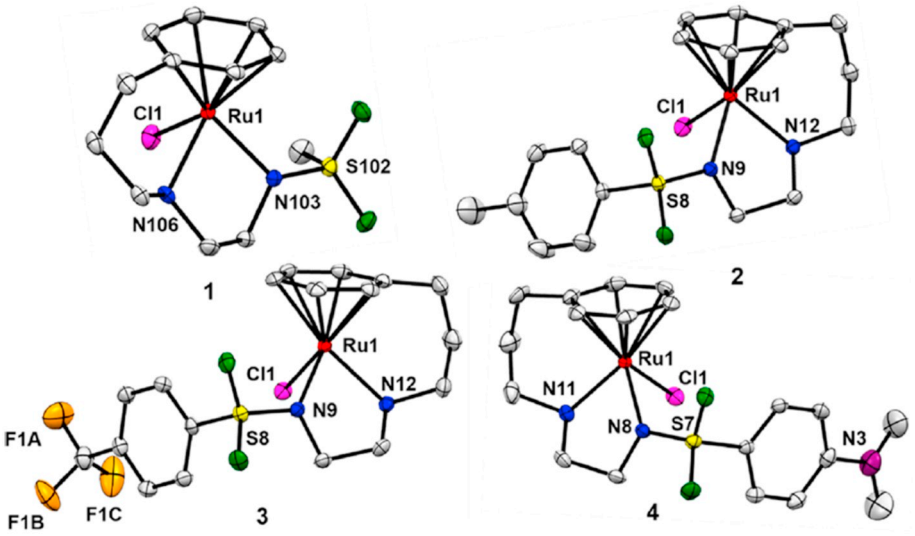

Fig. 4. ORTEP diagrams of [$Ru^{II}(\eta^6$-$Ph(CH_2)_3$-ethylenediamine-N-R)Cl] complexes, where R = methanesulfonyl (**1**), toluenesulfonyl (**2**), 4-trifluoromethylbenzenesulfonyl (**3**), and nitrobenzenesulfonyl (**4**). Reprinted with permission (CC-BY Licence) from Ref. [43]. Copyright 2018, American Chemical Society.

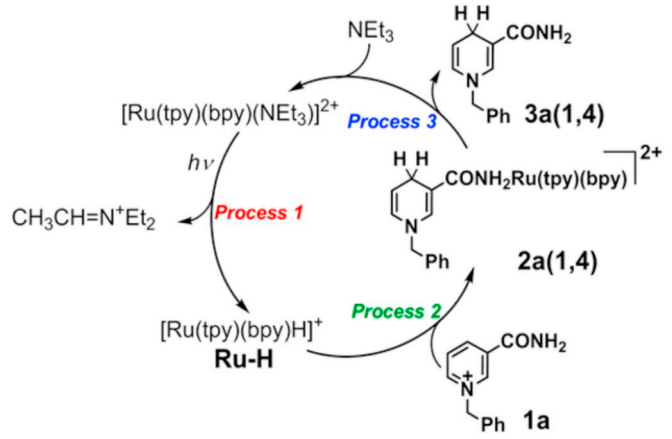

Scheme 4. Proposed mechanism of the photocatalytic regioselective reduction of BNA^+ (**1a**) by $[Ru(tpy)(bpy)(NEt_3)]^{2+}$ as a photoredox catalyst with NEt_3 as a reductant. Reprinted with permission from Ref. [46]. Copyright 2015, American Chemical Society.

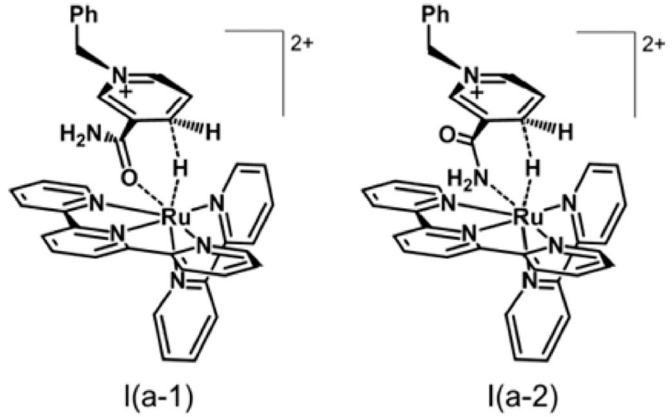

Fig. 5. Schematic structures in the transition state in the reaction of BNA^+ (**1a**) with Ru−H. Reprinted with permission from Ref. [46]. Copyright 2015, American Chemical Society.

coordinated –NH, followed by β-elimination of hydrogen from complex B to produce the Ir(III)-hydride complex (C), accompanied by CO_2 evolution [59]. The Ir(III)-hydride species (C) forms an adduct complex with NAD^+ (D) by hydrogen bonding between the carbamoyl group and the amide proton and also an interaction between the hydride ligand and the C-4 position of NAD^+ [59]. In adduct complex D, NAD^+ is regioselectively hydrogenated to liberate 1,4-NADH, accompanied by regeneration of the iridium(III)-aqua complex A [59]. The Ir(III) complex, [Cp*Ir(pica)Cl] also acts as an effective catalyst for water oxidation driven by cerium ammonium nitrate (CAN) and $NaIO_4$ [59].

An Ir(III)-hydride complex, $[Cp^*Ir^{III}(bpy)(H)]^+$, undergoes hydride transfer to 1-methylniconinamide cation (MNA^+) to produce 1,4-dihydro-1-methylnicotinamide MNA-H regioselectively under dark (Scheme 7) [60]. Under photoirradiation, 1,6-reduced MNA−H′ (52%) was produced and the doubly reduced product, 1,4,5,6-tetrahydro-1-methylnicotinamide (MNA−H_3), was also obtained in the presence of excess $[Cp^*Ir(bpy)(H)]^+$ at prolonged irradiation time (Scheme 7) [60].

5. Iron complex catalysts

Fe(II)-hydride Cp*(P−P)FeH complexes, Cp*(dppe)FeH (dppe = 1,2-$C_2H_4(PPh_2)_2$; **1H**) and its analogues [Cp*(dppbz)FeH (dppbz = 1,2-$C_6H_4(PPh_2)_2$; **2H**) and Cp*(dppm)FeH (dppm = $Ph_2PCH_2PPh_2$; **3H**)], can also reduce BNA^+ in CD_2Cl_2/CD_3CN(v/v 2:1) at room temperature to produce 1,4-BNAH (yield > 90%) and 1,6-BNAH (yield < 10%) (pathway *i* in Scheme 8) [61]. During the hydride-transfer reaction from **2H** to BNA^+, both 1,4-BNAH and 1,6-BNAH products increased slowly [62,63]. When the amount of reduced BNAH reached a plateau, the isomerization from 1,6-BNAH to 1,4-BNAH occurred, suggesting that the 1,4-BNAH product is more stable thermally [62,63].

When BNA^+ was replaced by 9-substituted 10-methylacridinium ($Acr(R_2)^+$; R_2 = Ph or H) ions, treatment of the Cp*(P−P)FeH (**1H**−**3H**) with $AcrH^+$ in CD_2Cl_2/MeCN (v/v 100:1) resulted in formation of organoiron products of $[Cp^*(P-P)Fe^{II}(NCMe)]^+$ and acridine dimer $(AcrH)_2$, accompanied by hydrogen evolution (pathway *ii* in Scheme 8) [61]. In this case, electron transfer from $Cp^*(P-P)Fe^{II}H$ to $AcrH^+$ occurs first to produce $[Cp^*(P-P)Fe^{III}H]^+$ and $AcrH^•$ [61]. The disproportionation of $[Cp^*(P-P)Fe^{III}H]^+$ produces H_2 and $[Cp^*(P-P)Fe^{II}(NCMe)]^+$ [61]. On the other hand, $AcrH^•$ dimerized to produce the acridine dimer $(AcrH)_2$ [61,64].

Hydride transfer from an iron(II)-hydride complex, $Cp^*(Ph_2PN^tBuPPh_2)Fe^{II}H$ ($Ph_2PN^tBuPPh_2$ = *N,N*-bis(diphenylphosphanyl)*tert*-butylamine, **1-H** in Scheme 9), to BNA^+ in MeCN afforded $[Cp^*(Ph_2PN^tBuPPh_2)Fe^{II}(NCMe)]^+$ ($[\mathbf{1}(NCMe)]^+$) and BNAH (Scheme 9) [65]. In THF, reaction of **1-H** with BNA^+ under high pressure of nitrogen (60 psi) affords the iron (II)-nitrogen complex $[Cp^*(Ph_2PN^tBuPPh_2)Fe^{II}(N_2)]^+$ ($[\mathbf{1}\text{-}\mathbf{N_2}]^+$) and BNAH [65]. In CH_2Cl_2, $[\mathbf{1}\text{-}\mathbf{N_2}]^+$ catalyzed the conversion of **1-H** to $Cp^*(Ph_2PN^tBuPPh_2)Fe^{II}Cl$ (**1-Cl**), accompanied by generation of H_2

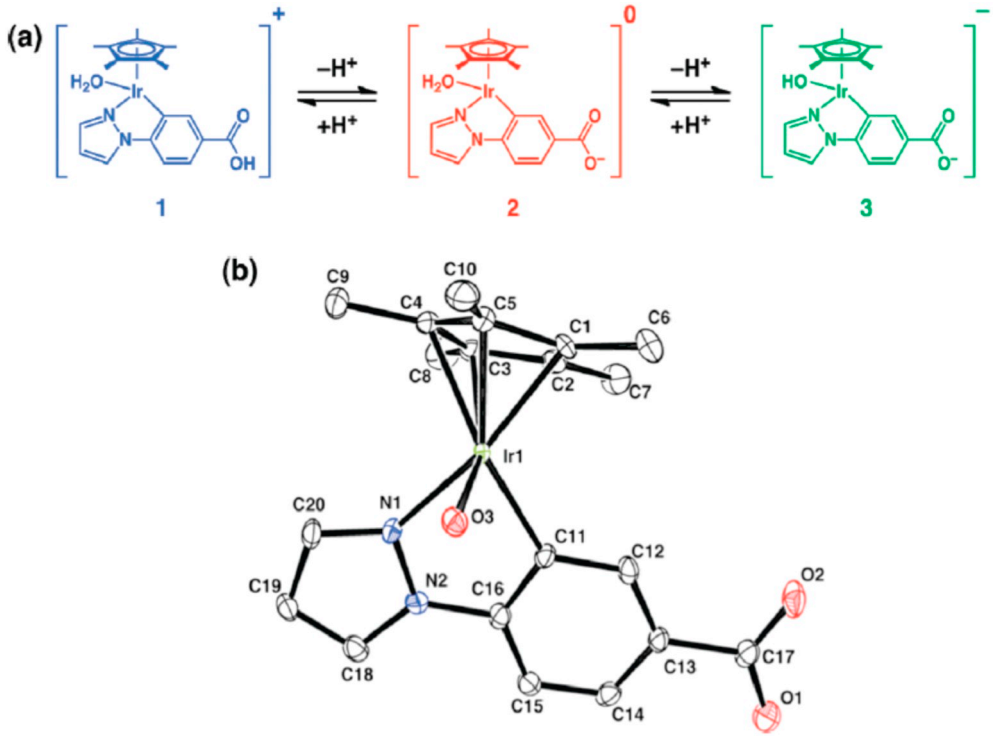

Fig. 6. (a) Iridium(III)-aqua complexes in acid-base equilibria. (b) Crystal structure of **2**. Reprinted with permission from Ref. [50]. Copyright 2011, American Chemical Society. (For interpretation of the references to colour in this figure legend, the reader is referred to the web version of this article.)

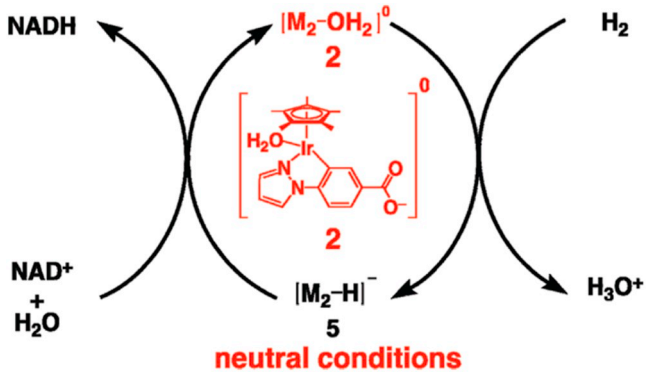

Scheme 5. Catalytic cycle of regioselective reduction of NAD^+ by H_2 using a [C,N] cyclometalated organoiridium complex as a redox catalyst. Reprinted with permission from Ref. [50]. Copyright 2011, American Chemical Society.

(Scheme 9), which hampers the expected hydride transfer reaction [65]. However, the hydride-transfer reaction in the presence of MeCN in THF, CH_2Cl_2, or benzene occurred always to yield BNAH and [**1**(NCMe)]$^+$ [65].

6. Artificial photosynthesis for recycle of NADPH

The photocatalytic reduction of NAD^+ to NADH has been combined with enzymatic reduction of CO_2 to mimic the function of the chloroplast, which is the energy conversion center of natural photosynthesis [66]. The chloroplast employs thylakoids to couple photoreaction and bioreaction, which can convert 100–120 Gts of carbon into biomass per year by harvesting 130 tW of solar energy as shown in Fig. 7, where PS II and PS I absorb visible light to generate electrons and holes [67,68]. The electrons are transferred to the stromal side of the thylakoid membrane through the electron transfer chain, and then transduced into biomass through NADPH in the Calvin cycle [67,68]. The holes left on the luminal side of the thylakoid membrane oxidize water into oxygen and protons [67,68].

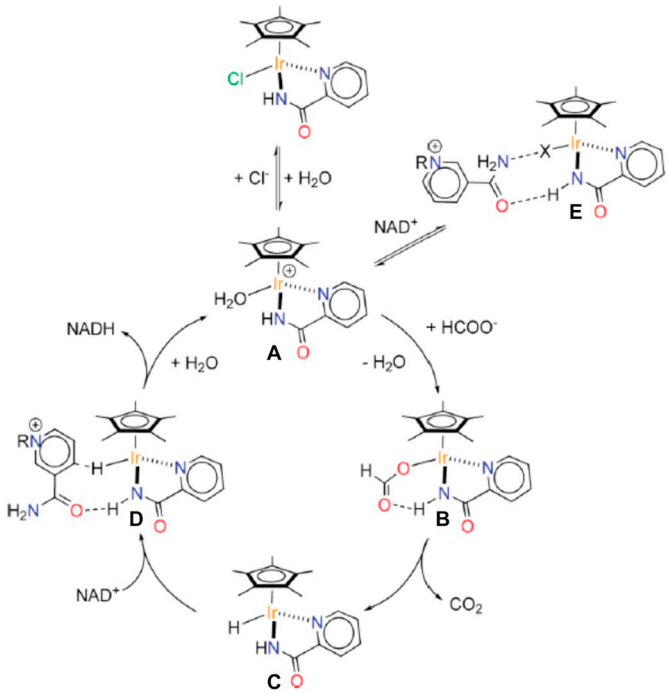

Scheme 6. Catalytic cycle of the regioselective reduction of NAD^+ with potassium formate (HCO_2K) by [Cp*Ir(pica)Cl]. Reprinted with permission from Ref. [59]. Copyright 2017, American Chemical Society.

An artificial thylakoid was constructed by decorating the inner wall of protamine-titania (PTi) microcapsules with cadmium sulfide quantum dots (CdS QDs) for the photobiocoupled reduction of carbon dioxide (CO_2) via a single enzyme (formate dehydrogenase) and multiple enzymes (formate/formaldehyde/alcohol dehydrogenases) as shown in Fig. 7b [66]. CdS QDs on the capsule wall absorb visible light

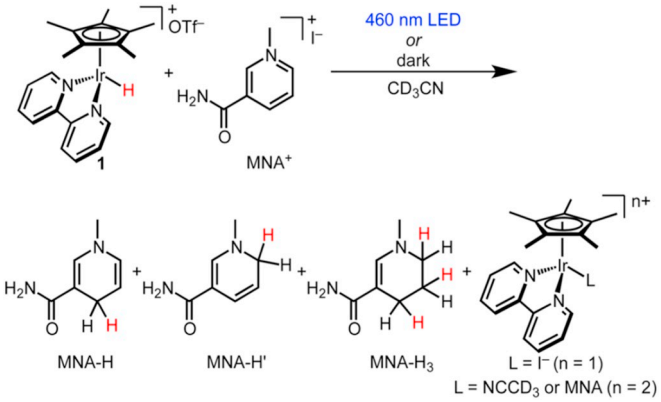

Scheme 7. Hydride transfer from Ir(III)-hydride complex, $[Cp^*Ir^{III}(bpy)(H)](OTf)$, to MNA^+ under photoirradiation (visible light) [60]. Reprinted with permission from Ref. [60]. Copyright 2014, American Chemical Society.

to generate electrons and holes [66]. The electrons are transferred to the outer surface of the capsule wall through the heterostructure of CdS and amorphous titania, and then transduced to formic acid through reduced β-nicotinamide adenine dinucleotide (NADH), which was produced by reduction of NAD^+ with $[Cp^*Rh^{III}(bpy)H_2O]^{2+}$, by formate dehydrogenase from *Candida boidinii* (CbFDH) [66]. The holes left on the inner surface of the capsule wall oxidize triethanolamine (TEOA) [66]. The NADH regeneration rate was determined to be $4226 \pm 121\ \mu mol\ g^{-1}\ h^{-1}$ and the optimized yield was $93.03 \pm 3.84\%$ based on TEOA [66]. The formation rates of formate and methanol were determined to be 1500 and $99\ \mu M\ h^{-1}$ with a single enzyme and multiple enzymes, respectively [66].

7. Concluding remarks

In this review, we have provided an overview on the thermal and photodriven catalytic regioselective reduction of $NAD(P)^+$ and biomimetic model compounds to produce 1,4-NAD(P)H and its analogs. The formation of metal-hydride intermediates is the bottom line of the NAD^+ reduction to afford NADH. Interactions of the carbamoyl group

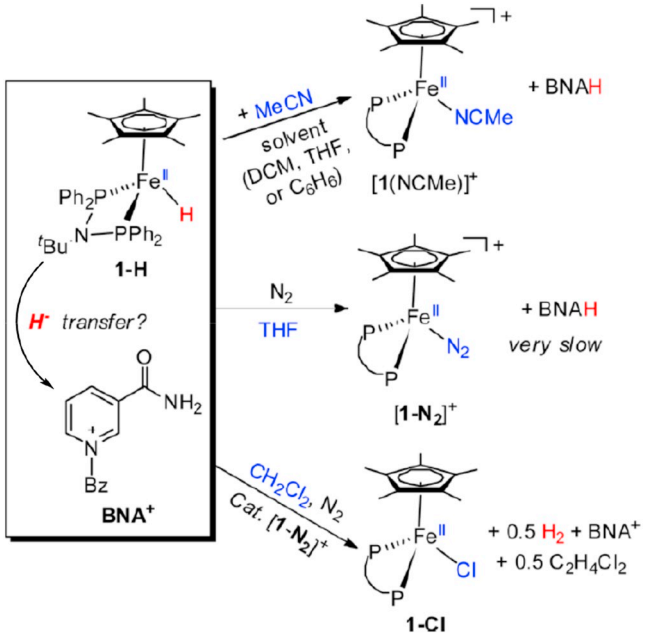

Scheme 9. Reaction products obtained in the hydride transfer from $Cp^*(Ph_2PN^tBuPPh_2)Fe^{II}H$ to BNA^+ in MeCN, THF and CH_2Cl_2. Reprinted with permission from Ref. [65]. Copyright 2017, American Chemical Society.

(or NH_2 group) of NAD^+ and its analogs with the metal centers of Rh(III)-, Ru(III)- and Ir(III)-hydride complexes together with an interaction between the hydride ligand and the C-4 position of the pyridinium result in the regioselective reduction of NAD^+ to 1,4-NADH. In the case of Fe(II)-hydride complexes, however, an NAD^+ biomimetic model compound (BNA^+) is reduced by the hydrides to produce not only 1,4-BNAH but also 1,6-BNAH, which is finally isomerized to 1,4-BNAH. When 10-methylacridinium ion ($AcrH^+$) was employed as an NADH analog, $AcrH^+$ was reduced by Fe(II)-hydride complexes via electron transfer to yield the dimer $[(AcrH)_2]$, accompanied by generation of hydrogen molecule (H_2). The catalytic regioselective reduction of

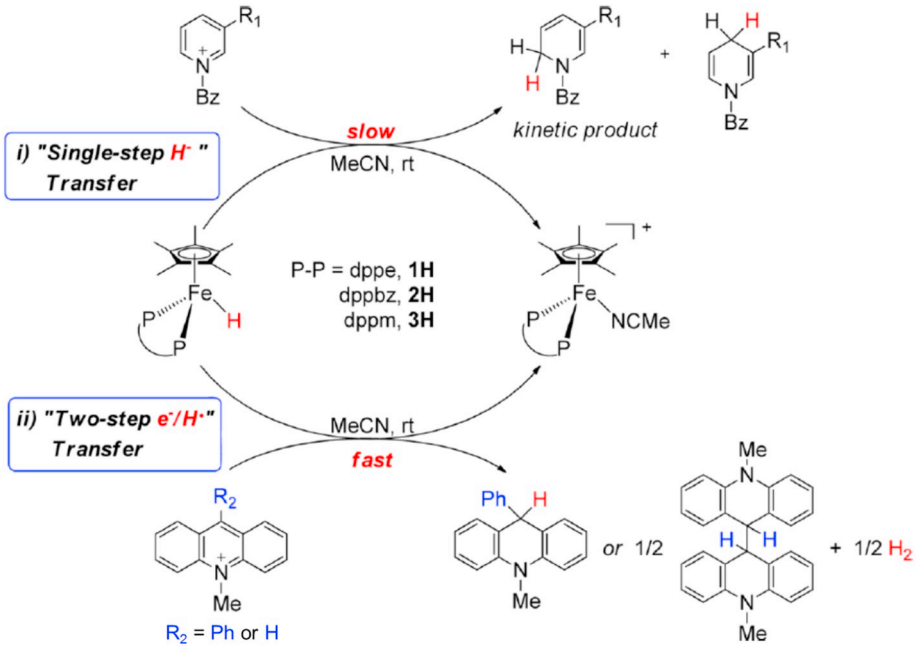

Scheme 8. Mechanisms of hydride transfer from Cp*(P—P)FeH to 3-R_1-*N*-benzylpyridinium and 9-R_2-10-methylacridinium (R_2 = Ph or H) ions. Reprinted with permission from Ref. [61]. Copyright 2016, American Chemical Society.

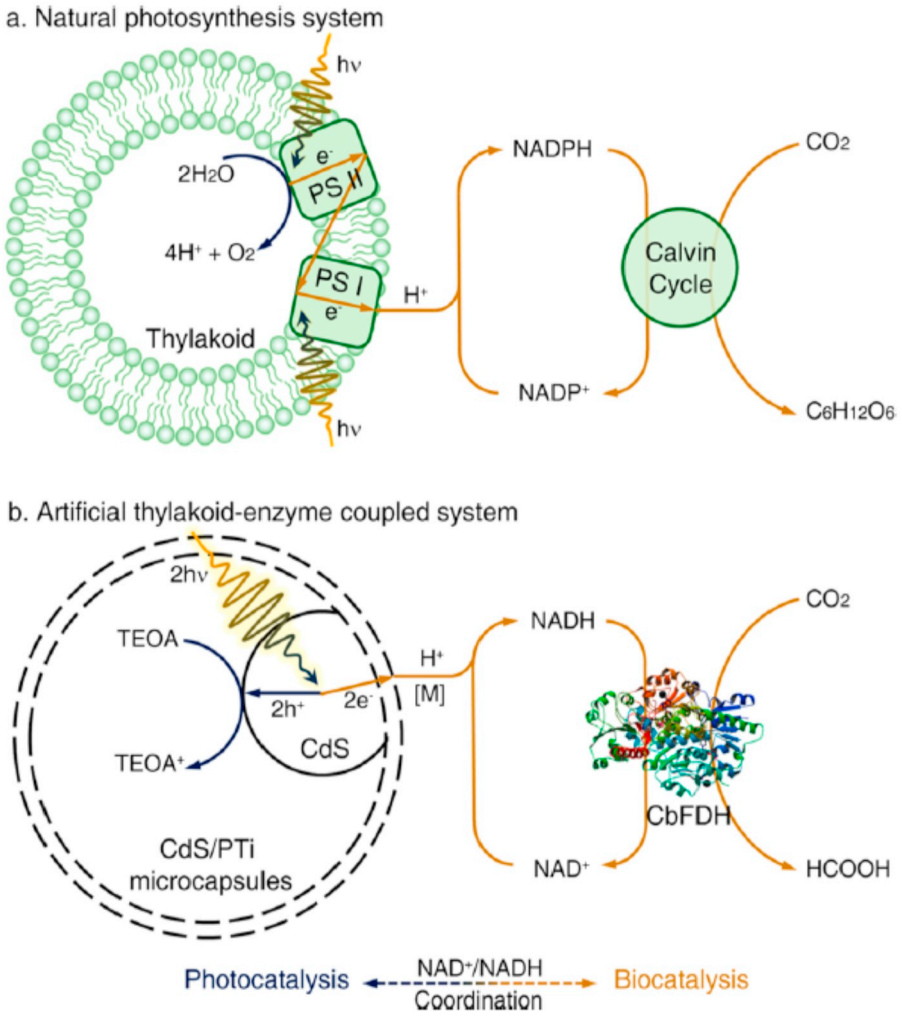

Fig. 7. Comparison of (a) natural photosynthesis with (b) artificial thylakoid-enzyme coupled system. Reprinted with permission from Ref. [66]. Copyright 2019, American Chemical Society.

NAD^+ to NADH has been combined with enzymatic reduction of CO_2 to mimic the function of the chloroplast. It is highly desired to develop artificial photosynthetic systems, in which electrons and protons are taken from water to reduce $NAD(P)^+$ to NAD(P)H that reduces CO_2 to produce liquid fuels.

Abbreviations

NAD^+	nicotinamide adenine dinucleotide
$NADP^+$	nicotinamide adenine dinucleotide phosphate
NADH	dihydronicotinamide adenine dinucleotide
NADPH	dihydronicotinamide adenine dinucleotide phosphate
BNAH	1-benzyl-1,4-dihydronicotinamide
BNA^+	1-benzylnicotinamidium cation
SCE	saturated calomel electrode
MWCNT	multiwall carbon nanotube
CF-CNT	MWCNT-functionalized carbon felt electrode
bpy	2,2′-bipyridine
TEOA	triethanolamine
OTf^-	trifluoromethanesulfonate ($CF_3SO_3^-$)
$g\text{-}C_3N_4$	graphitic carbon nitride
$g\text{-}C_3N_4@\alpha\text{-}Fe_2O_3/C$	a nanoshell with two moieties of α-Fe_2O_3 and carbon (C) in situ formed on the surface of a $g\text{-}C_3N_4$ core
LED	light emitting diode
TON	turnover number
TOF	turnover frequency
Cp^*	pentamethylcyclopentadienyl anion
tpy	2,2′:6″,2″-terpyridine
QDs	quantum dots

Declaration of Competing Interest

The authors declare that there are no conflicts of interest.

Acknowledgements

The authors gratefully acknowledge the contributions of their collaborators and coworkers mentioned in the cited references, and financial supports by a SENTAN project from JST and JSPS KAKENHI (Grant Numbers 16H02268 to S.F.) from MEXT, Japan and by the NRF of Korea through CRI (NRF-2012R1A3A2048842 to W.N.), GRL (NRF-2010-00353 to W.N.), and Basic Science Research Program (2017R1D1A1B03029982 to Y.-M.L. and 2017R1D1A1B03032615 to S.F.).

References

[1] F. Nastri, M. Chino, O. Maglio, A. Bhagi-Damodaran, Y. Lu, A. Lombardi, Chem. Soc. Rev. 45 (2016) 5020–5054.
[2] X. Huang, J.T. Groves, Chem. Rev. 118 (2018) 2491–2553.
[3] F. Schwizer, Y. Okamoto, T. Heinisch, Y. Gu, M.M. Pellizzoni, V. Lebrun, R. Reuter, V. Kohler, J.C. Lewis, T.R. Ward, Chem. Rev. 118 (2018) 142–231.
[4] J. Dong, E. Fernández-Fueyo, F. Hollmann, C.E. Paul, M. Pesic, S. Schmidt, Y. Wang,

S. Younes, W. Zhang, Angew. Chem. Int. Ed. 57 (2018) 9238–9261.
[5] S. Hirota, Y.W. Lin, J. Biol. Inorg. Chem. 23 (2018) 7–25.
[6] Y.W. Lin, Coord. Chem. Rev. 336 (2017) 1–27.
[7] N.D. Fessner, ChemCatChem 11 (2019) 2226–2242.
[8] M. Guo, T. Corona, K. Ray, W. Nam, ACS Cent. Sci. 5 (2019) 13–28.
[9] F. Rudroff, Curr. Opin. Chem. Biol. 49 (2019) 84–90.
[10] R.A. Sheldon, D. Brady, Chem. Commun. 54 (2018) 6088–6104.
[11] M. Polakovič, J. Švitel, M. Bučko, J. Filip, V. Neděla, M.B. Ansorge-Schumacher, P. Gemeiner, Biotechnol. Lett. 39 (2017) 667–683.
[12] N. Ladkau, A. Schmid, B. Bühler, Curr. Opin. Biotechnol. 30 (2014) 178–189.
[13] M. Schrewe, M.K. Julsing, B. Bühler, A. Schmid, Chem. Soc. Rev. 42 (2013) 6346–6377.
[14] M. Karasawa, J.K. Stanfield, S. Yanagisawa, O. Shoji, Y. Watanabe, Angew. Chem. Int. Ed. 57 (2018) 12264–12269.
[15] L. Lauterbach, O. Lenz, K.A. Vincent, FEBS J. 280 (2013) 3058–3068.
[16] X. Wang, T. Saba, H.H.P. Yiu, R.F. Howe, J.A. Anderson, J. Shi, Chem 2 (2017) 621–654.
[17] T. Quinto, V. Köhler, T.R. Ward, Top. Catal. 57 (2014) 321–331.
[18] R.H. Fish, J. Organomet. Chem. 782 (2015) 3–16.
[19] F. Hollmann, I.W.C.E. Arends, K. Buehler, ChemCatChem 2 (2010) 762–782.
[20] C. Rodriguez, I. Lavandera, V. Gotor, Curr. Org. Chem. 16 (2012) 2525–2541.
[21] H. Wu, C. Tian, X. Song, C. Liu, D. Yang, Z. Jiang, Green Chem. 15 (2013) 1773–1789.
[22] A. Mcskimming, S.B. Colbran, Chem. Soc. Rev. 42 (2013) 5439–5488.
[23] S. Fukuzumi, Y.-M. Lee, W. Nam, ChemPhotoChem 2 (2018) 121–135.
[24] W. Zhang, F. Hollmann, Chem. Commun. 54 (2018) 7281–7289.
[25] S. Morra, A. Pordea, Chem. Sci. 9 (2018) 7447–7454.
[26] C.F. Megarity, B. Siritanaratkul, R.S. Heath, L. Wan, G. Morello, S.R. FitzPatrick, R.L. Booth, A.J. Sills, A.W. Robertson, J.H. Warner, N.J. Turner, F.A. Armstrong, Angew. Chem. Int. Ed. 58 (2019) 4948–4952.
[27] M. Silvi, P. Melchiorre, Nature 554 (2018) 41–49.
[28] R. Wienkamp, E. Steckhan, Angew. Chem. Int. Ed. Engl. 21 (1982) 782–783.
[29] L. Zhang, N. Vilà, G.W. Kohring, A. Walcarius, M. Etienne, ACS Catal. 7 (2017) 4386–4394.
[30] L. Zhang, M. Etienne, N. Vilà, T.X.H. Le, G.W. Kohring, A. Walcarius, ChemCatChem 10 (2018) 4067–4073.
[31] R. Wienkamp, E. Steckhan, Angew. Chem. Int. Ed. Engl. 22 (1983) 497.
[32] H.C. Lo, O. Buriez, J.B. Kerr, R.H. Fish, Angew. Chem. Int. Ed. 38 (1999) 1429–1432.
[33] T. Kuwabara, R. Tezuka, M. Ishikawa, T. Yamazaki, S. Kodama, Y. Ishii, Organometallics 37 (2018) 1829–1832.
[34] Q. Pan, H. Liu, Y. Zhao, S. Chen, B. Xue, X. Kan, X. Huang, J. Liu, Z. Li, ACS Appl. Mater. Interfaces 11 (2019) 2740–2744.
[35] W.D. Jones, V.L. Kuykendall, A.D. Selmeczy, Organometallics 10 (1991) 1577–1586.
[36] T. Saba, J.W.H. Burnetta, J. Li, X. Wang, J.A. Andersona, P.N. Kechagiopoulos, X. Wang, Catal. Today (2019), https://doi.org/10.1016/j.cattod.2019.01.049.
[37] D. Yang, Y. Zhang, H. Zou, S. Zhang, Y. Wu, Z. Cai, J. Shi, Z. Jiang, ACS Sustain. Chem. Eng. 7 (2019) 285–295.
[38] D. Yang, H. Zou, Y. Wu, J. Shi, S. Zhang, X. Wang, P. Han, Z. Tong, Z. Jiang, Ind. Eng. Chem. Res. 56 (2017) 6247–6255.
[39] J. Meng, Y. Tian, C. Li, X. Lin, Z. Wang, L. Sun, Y. Zhou, J. Li, N. Yang, Y. Zong, F. Li, Y. Cao, H. Song, Catal. Sci. Technol. 9 (2019) 1911–1921.
[40] E.J. Son, Y.W. Lee, J.W. Ko, C.B. Park, ACS Sustain. Chem. Eng. 7 (2019) 2545–2552.
[41] Y. Wu, J. Ward-Bond, D. Li, S. Zhang, J. Shi, Z. Jiang, ACS Catal. 8 (2018) 5664–5674.
[42] K.T. Oppelt, J. Gasiorowski, D.A.M. Egbe, J.P. Kollender, M. Himmelsbach, A.W. Hassel, N.S. Sariciftci, G. Knör, J. Am. Chem. Soc. 136 (2014) 12721–12729.
[43] F. Chen, I. Romero-Canelón, J.J. Soldevila-Barreda, J.I. Song, J.P.C. Coverdale, G.J. Clarkson, J. Kasparkova, A. Habtemariam, M. Wills, V. Brabec, P.J. Sadler, Organometallics 37 (2018) 1555–1566.
[44] O. Ishitani, N. Inoue, K. Koike, T. Ibusuki, J. Chem. Soc. Chem. Commun. (1994) 367–368.
[45] Y. Matsubara, H. Konno, A. Kobayashi, O. Ishitani, Inorg. Chem. 48 (2009) 10138–10145.
[46] K. Koga, Y. Matsubara, T. Kosaka, K. Koike, T. Morimoto, O. Ishitani, Organometallics 34 (2015) 5530–5539.
[47] A. Kobayashi, H. Konno, K. Sakamoto, A. Sekine, Y. Ohashi, M. Iida, O. Ishitani, Chem. Eur. J. 11 (2005) 4219–4226.
[48] A. Kobayashi, R. Takatori, I. Kikuchi, H. Konno, K. Sakamoto, O. Ishitani, Organometallics 20 (2001) 3361–3363.
[49] Y. Matsubara, K. Koga, A. Kobayashi, H. Konno, K. Sakamoto, T. Morimoto, O. Ishitani, J. Am. Chem. Soc. 132 (2010) 10547–10552.
[50] Y. Maenaka, T. Suenobu, S. Fukuzumi, J. Am. Chem. Soc. 134 (2012) 367–374.
[51] Y. Maenaka, T. Suenobu, S. Fukuzumi, Energy Environ. Sci. 5 (2012) 7360–7367.
[52] Y. Maenaka, T. Suenobu, S. Fukuzumi, J. Am. Chem. Soc. 134 (2012) 9417–9427.
[53] K. Sordakis, C. Tang, L.K. Vogt, H. Junge, P.J. Dyson, M. Beller, G. Laurenczy, Chem. Rev. 118 (2018) 372–433.
[54] A. Kumar, S. Semwal, J. Choudhury, ACS Catal. 9 (2019) 2164–2168.
[55] S. Fukuzumi, Joule 1 (2017) 689–738.
[56] W.H. Wang, Y. Himeda, J.T. Muckerman, G.F. Manbeck, E. Fujita, Chem. Rev. 115 (2015) 12936–12973.
[57] S. Fukuzumi, T. Suenobu, Dalton Trans. 42 (2013) 18–28.
[58] X. Shao, X. Yang, J. Xu, S. Liu, S. Miao, X. Liu, X. Su, H. Duan, Y. Huang, T. Zhang, Chem 5 (2019) 693–705.
[59] A. Bucci, S. Dunn, G. Bellachioma, G.M. Rodriguez, C. Zuccaccia, C. Nervi, A. Macchioni, ACS Catal. 7 (2017) 7788–7796.
[60] S.M. Barrett, C.L. Pitman, A.G. Walden, A.J.M. Miller, J. Am. Chem. Soc. 136 (2014) 14718–14721.
[61] F. Zhang, J. Jia, S. Dong, W. Wang, C.H. Tung, Organometallics 35 (2016) 1151–1159.
[62] C.E. Paul, I.W.C.E. Arends, F. Hollmann, ACS Catal. 4 (2014) 788–797.
[63] W.S. Caughey, K.A. Schellenberg, J. Org. Chem. 31 (1966) 1978.
[64] S. Fukuzumi, T. Kitano, K. Mochida, J. Am. Chem. Soc. 112 (1990) 3246–3247.
[65] F. Zhang, X. Xu, Y. Zhao, J. Jia, C.H. Tung, W. Wang, Organometallics 36 (2017) 1238–1244.
[66] S. Zhang, J. Shi, Y. Sun, Y. Wu, Y. Zhang, Z. Cai, Y. Chen, C. You, P. Han, Z. Jiang, ACS Catal. 9 (2019) 3913–3925.
[67] R.E. Blankenship, D.M. Tiede, J. Barber, G.W. Brudvig, G. Fleming, M. Ghirardi, M.R. Gunner, W. Junge, D.M. Kramer, A. Melis, T.A. Moore, C.C. Moser, D.G. Nocera, A.J. Nozik, D.R. Ort, W.W. Parson, R.C. Prince, R.T. Sayre, Science 332 (2011) 805–809.
[68] J. Barber, Chem. Soc. Rev. 38 (2009) 185–196.